Electronic Supplementary Information

Experimental section

Materials

Ti_3AlC_2 was purchased from Laizhou KaiXi Ceramic Materials Company Ltd. Nafion (5 wt%) was purchased from Sigma-Aldrich Chemical Reagent Co., Ltd. Hydrochloric acid (HCl), and ethanol (C_2H_5OH) were purchased from Chengdu Kelong Chemical Reagent Factory. Manganese sulfate ($MnSO_4$), potassium permanganate ($KMnO_4$), Sodium salicylate ($C_7O_3H_5Na$), sodium hypochlorite (NaClO), sodium nitroferricyanide dihydrate ($C_5FeN_6Na_2O{\cdot}2H_2O$), para-(dimethylamino) benzaldehyde (p-$C_9H_{11}NO$), and hydrazine monohydrate ($N_2H_4{\cdot}H_2O$) were purchased from Aladdin Ltd. (Shanghai, China). The water used throughout all experiments was purified through a Millipore system. All chemicals were used as received without further purification.

Synthesis of $Ti_3C_2T_x$

$Ti_3C_2T_x$ was synthesized by etching of the MAX Ti_3AlC_2 material based on the previous report method.[1] Typically, 5.0 g Ti_3AlC_2 particles were immersed in 80 mL 40% HF solution under magnetic stirring at room temperature for 48 h. After corrosion, the resultant precipitates were repeatedly washed with deionized water and centrifuged at 3500 rpm for 5 min, until the supernatant reached a pH of approximate 6 and then washed by absolute ethanol at least three times. The acquired sediment was dried at room temperature for 90 h. Subsequently, 0.5 g of as-prepared $Ti_3C_2T_x$ powder was dispersed in 250 mL distilled water forming a suspension, deaerated with Ar, followed by sonication under for 1 h. Thereafter, the suspension was centrifuged at 3500 rpm for 1 h and the supernatant was collected.[2] Finally, the resulting product can be obtained by freeze-dried.

Synthesis of MnO_2-$Ti_3C_2T_x$

In the present work, MnO_2 was deposited over $Ti_3C_2T_x$ nanosheet by direct chemical synthesis.[3] Typically, 200 mg of $Ti_3C_2T_x$ were dispersed in 35 mL of an aqueous solution, containing 10 mM of $MnSO_4$, by sonication for 30 min. To allow impregnation of the $Ti_3C_2T_x$ by $MnSO_4$, the suspension was then maintained at a controlled temperature of 60 ºC for 30

min under magnetic stirring. A 150 mL aqueous solution containing 33 mM of $KMnO_4$ was previously heated at controlled 60 ºC, and then slowly added to the agitated suspension. This mixture was maintained at 60 ºC under agitation for 15 min and then washed, filtered and vacuum dried at 80 ºC for approximately 10 h. For comparison, pure MnO_2 was also prepared by a similar procedure.

Preparation of MnO_2-$Ti_3C_2T_x$/CP electrode

MnO_2-$Ti_3C_2T_x$/CP was prepared as following: First, 5 mg of MnO_2-$Ti_3C_2T_x$ composites and 20 μL of Nafion solution (5 wt%) were dispersed in 980 μL mixed solution contain ethanol and H_2O (V:V=2:1) by 1 h sonication to form a homogeneous ink. Then 20 μL catalyst ink was loaded on a 1×1 cm^2 carbon paper (CP) and dried under ambient condition for measurement.

Characterizations

XRD patterns were obtained from a Shimazu XRD-6100 diffractometer with Cu Kα radiation (40 kV, 30 mA) of wavelength 0.154 nm (Japan). TEM images were obtained from a Zeiss Libra 200FE transmission electron microscope operated at 200 kV. XPS measurements were performed on an ESCALABMK II X-ray photoelectron spectrometer using Mg as the exciting source. The UV-Vis absorbance spectra were measured on a SHIMADZU UV-1800 UV-Vis spectrophotometer. The ion chromatography data were collected on Thermofisher ICS 5000 plus using the dual temperature heater, injection valve, conductivity detector, AERS 500 Anions suppressor. Brunauer–Emmett–Teller (BET) specific surface areas were measured by using Autosorb-IQ-MP-C system (Quantachrome, USA).

Electrochemical measurements

The electrochemical performance measurement was performed in a two-compartment cell separated by Nafion membrane using a CHI 660E electrochemical analyzer (CHI Instruments, Inc., Shanghai). Before NRR test, Nafion membrane was protonated by boiling in water a H_2O_2 for 1 h, then in water for another hour, followed by 1 h in 0.5 M H_2SO_4, and finally for 1 h in water. All steps were performed at 80 °C. The MnO_2-$Ti_3C_2T_x$/CP was used as the working electrode, a graphite rod as the counter electrode and Ag/AgCl electrode as the

reference. All experiments were performed at ambient conditions. Before the NRR measurements, the HCl electrolyte (0.1 M) was bubbled with high-purity N_2 (99.999%) for 20 min. For N_2 reduction experiments, potentiostatic test was conducted in N_2-saturated 0.1 M HCl solution. N_2 was continuously fed into the cathodic compartment with a properly positioned sparger during the experiments. All potentials reported in this work were calibrated to RHE, using the following equation:

$$E\ (RHE) = E\ (Ag/AgCl) + 0.059 \times pH + E^{\circ}\ (Ag/AgCl)$$

Determination of NH_3

NH_3 concentration was detected by the indophenol blue method.[4] In detail, 2 mL electrolyte was obatined from the cathodic chamber, and then 2 mL of 1 M NaOH solution (contains 5 wt% salicylic acid and 5 wt% sodium citrate) was added into this solution. Subsequently, 1 mL of 0.05 M sodium hypochlorite and 0.2 mL of sodium nitroferricyanide (1 wt%) were add into the above solution. After standing at room temperature for 2 h, the UV-Vis absorption absorption spectrum was measured at a wavelength of 655 nm. The concentration-absorbance curves were calibrated using standard NH_4Cl solution (0.1 M HCl solution as mother solution) with a serious of concentrations. The fitting curve ($y = 0.359\ x + 0.051$, $R^2 = 0.999$) shows good linear relation of absorbance value with NH_3 concentration by three times independent calibrations. The NH_3 concentration was calculated from the calibration curve, and the rate of NH_3 yield was calculated using the following equation:

$$V_{NH3}\ (\mu g\ h^{-1}\ mg_{cat.}^{-1}) = (c_{NH3} \times V) / (17 \times t \times m_{cat.})$$

where c_{NH3} ($\mu g\ mL^{-1}$) is the measured NH_3 concentration, V (mL) is the volume of electrolyte (in our work 35 mL), t (s) is the reduction reaction time and $m_{cat.}$ (mg) is the mass loading of catalyst on CP

Determination of N_2H_4

Concentration of N_2H_4 in the electrolyte was determined by the method of Watt and Chrisp.[5] Typically, a mixture solution containing p-$C_9H_{11}NO$ (5.99 g), concentrated HCl (30 mL) and C_2H_5OH (300 mL) was used as a color reagent. In detail, 5 mL electrolyte removed from the cathodic chamber was added into 5mL above prepared color reagent and standing 15 min at room temperature. UV-Vis absorption spectra were measured at a wavelength of 455 nm. The

obtained calibration curve of N_2H_4 is y = 0.76 x + 0.04, R^2 = 0.999.

Calculations of FE

FE in 0.1 M HCl was calculated according to following equation:

$$FE = 3 \times F \times c_{NH3} \times V / (17 \times Q) \times 100\%$$

Where F is Faraday constant (96500 C mol^{-1}); Q (C) is the quantity of applied electricity.

DFT calculation

Spin-polarized density function theory (DFT) was employed in all computations using Vienna Ab-initio Simulation Package (VASP).[6] The electron exchange was described by the Perdew-Burke-Ernzerhof (PBE) function along with a generalized gradient approximation (GGA).[7,8] The projector augmented wave (PAW) method was used to describe the electron-ion interaction. The kinetic energy cutoff for plane wave was chosen as 400 eV.[9] The Brillouin zone was sampled by using a 3×3×1 k-points grid. Then the structures were optimized until the atomic energy reached an energy convergence threshold of 10^{-4} eV and the force of each atom was lower than the criterion of 0.05 eV/Å. The structure was modeled by using an unit cell of (110) surface of MnO_2 and a 3×1×1 supercell of Ti_3C_2 MXene. A vacuum space of 20 Å in the z-direction was introduced to eliminate the mutual effect of different layers.

The distal reaction pathway was utilized to investigate the reaction process of NRR. For each intermediate step, the change of Gibbs free energy, ΔG, was given by

$$\Delta G=\Delta E+\Delta ZPE-T\Delta S-eU \quad (1)$$

where Δ*E* is the difference of calculated DFT energy. *ZPE* is zero-point energy, which was calculated from the vibrational frequency. *T* is the temperature, used as 298.15 K. *eU* is the contribution of free energy from the electrode potential *U* in the proton transfer steps. Charge transfer analysis was performed by utilizing Bader Charge Analysis method.

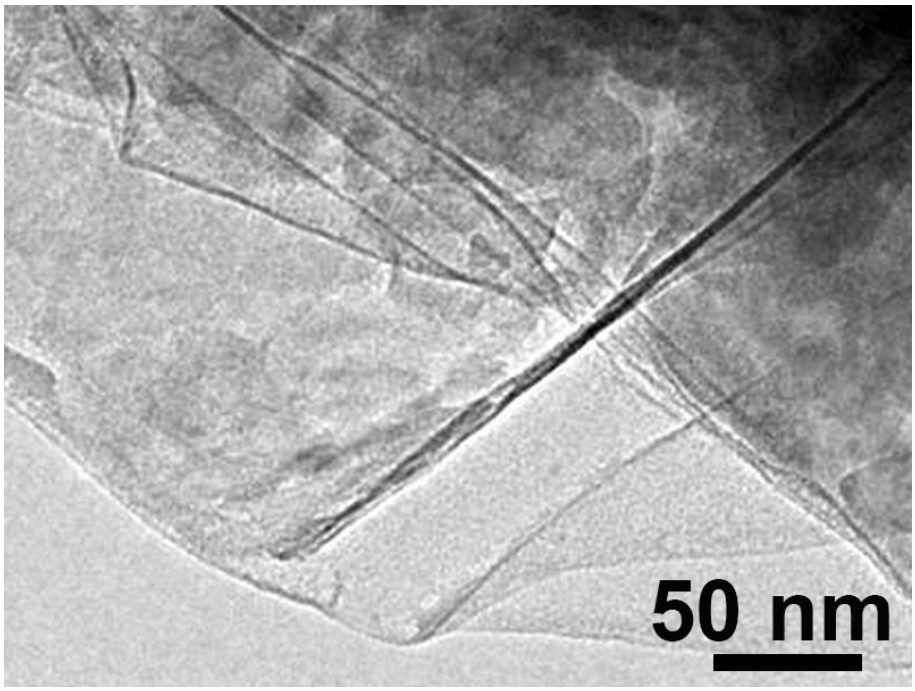

Fig. S1. TEM image of $Ti_3C_2T_x$ nanosheet.

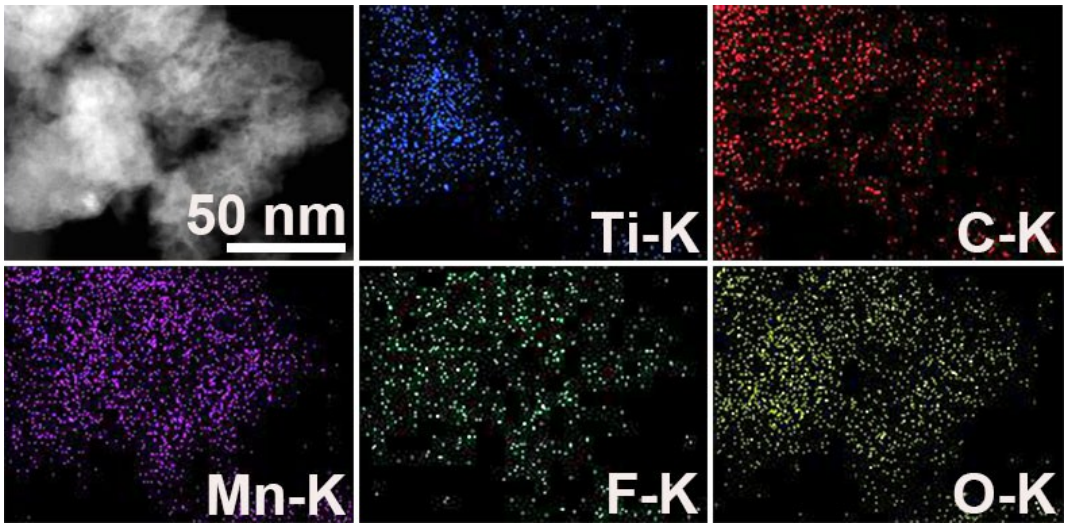

Fig. S2. TEM image and corresponding EDX elemental mapping images of Ti, C, Mn, F, and O for MnO_2-$Ti_3C_2T_x$.

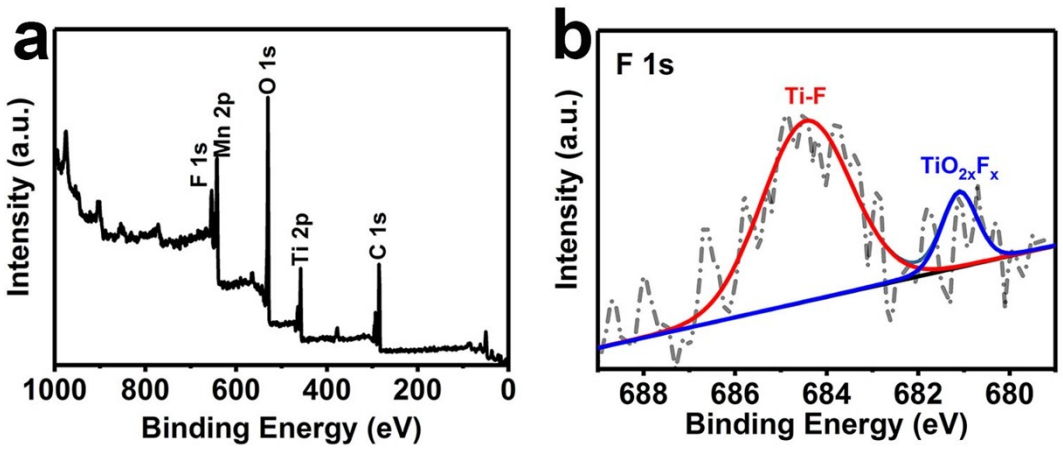

Fig. S3. (a) XPS survey spectrum of MnO_2-$Ti_3C_2T_x$ NS. (b) XPS spectrum for MnO_2-$Ti_3C_2T_x$ in the F 1s.

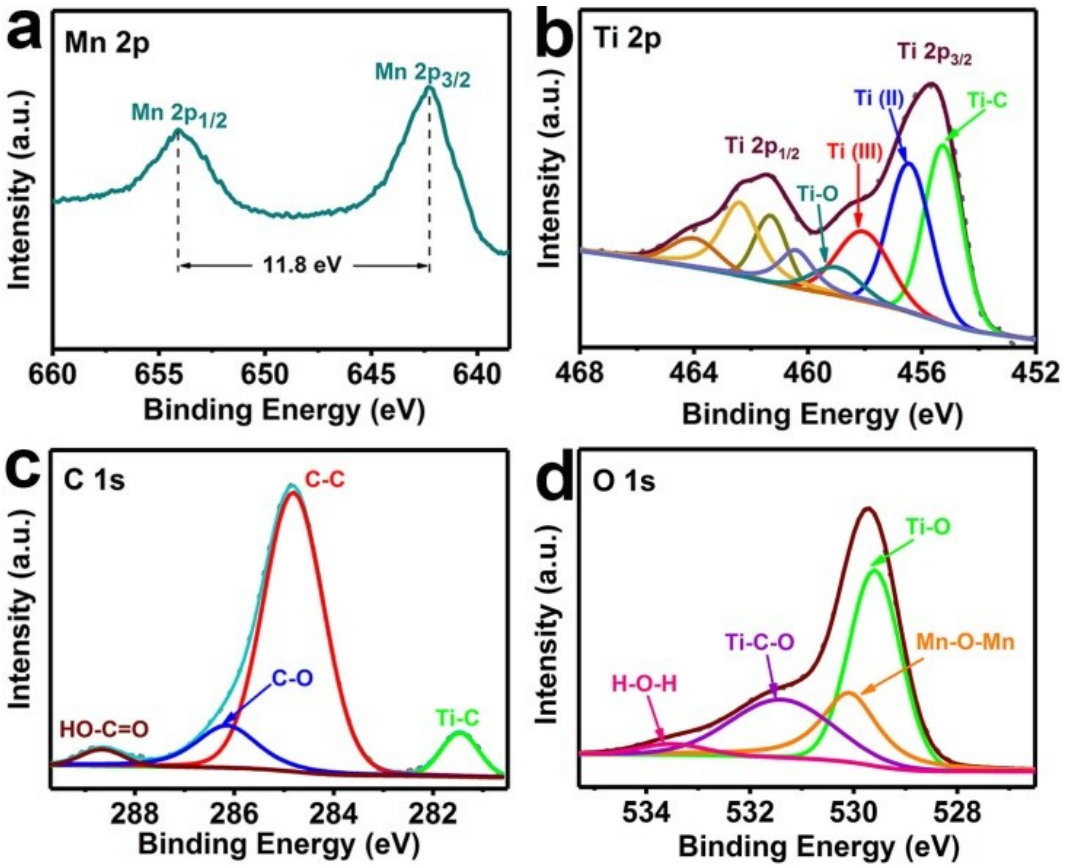

Fig. S4. XPS spectra for MnO_2-$Ti_3C_2T_x$ in the (a) Mn 2p, (b) Ti 2p, (c) C 1s, and (d) O 1s regions

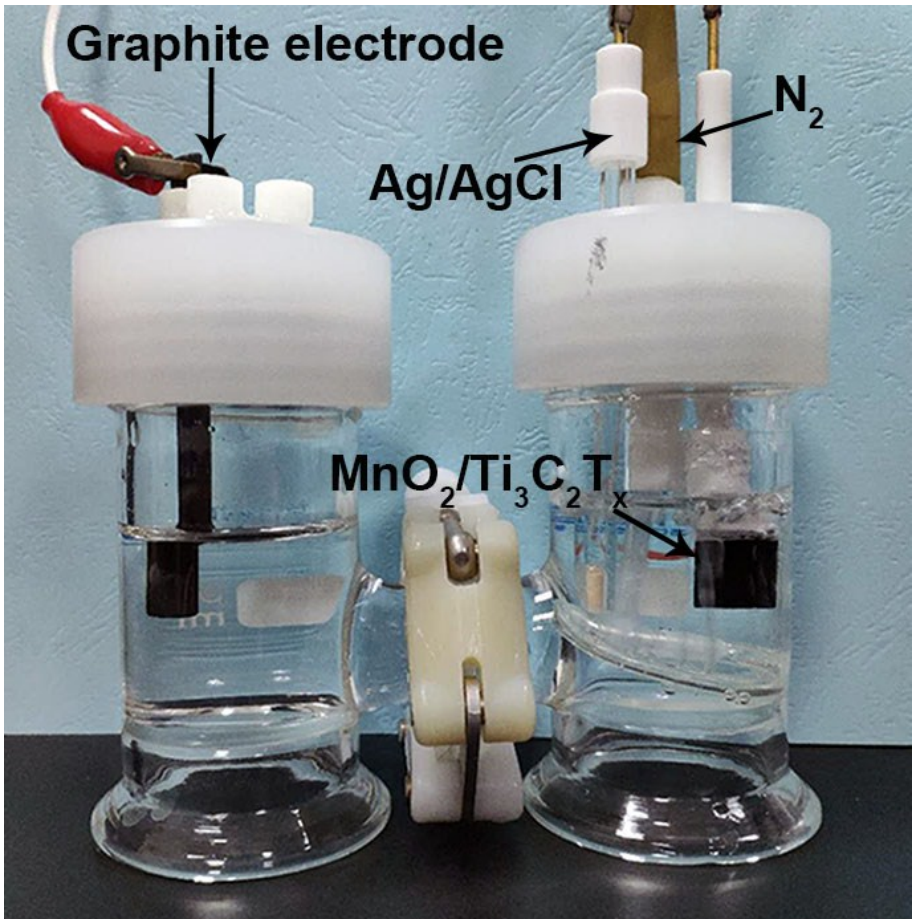

Fig. S5. Optical photograph of the reaction vessel.

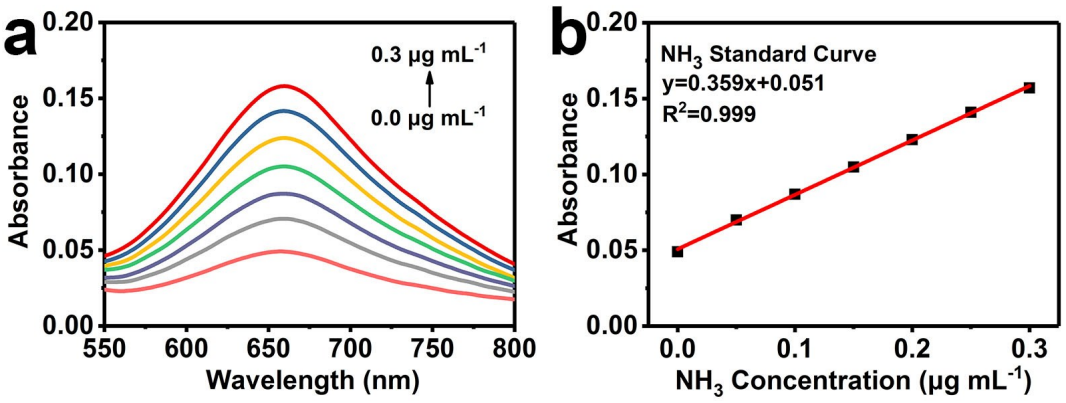

Fig. S6. (a) UV–Vis absorption spectra of various NH_3 concentrations after incubated for 2 h at room temperature. (b) Calibration curve used for calculation of NH_3 concentrations.

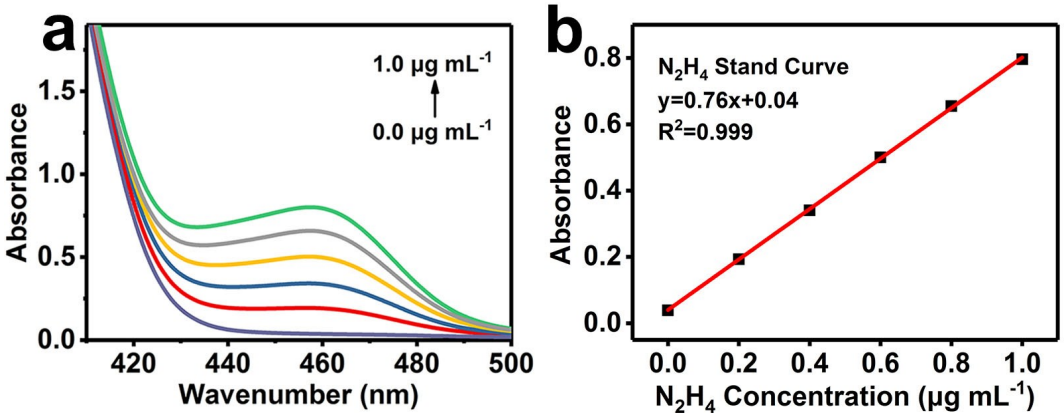

Fig. S7. (a) UV–Vis absorption spectra of various N_2H_4 concentrations after incubated for 20 min at room temperature. (b) Calibration curve used for calculation of N_2H_4 concentrations.

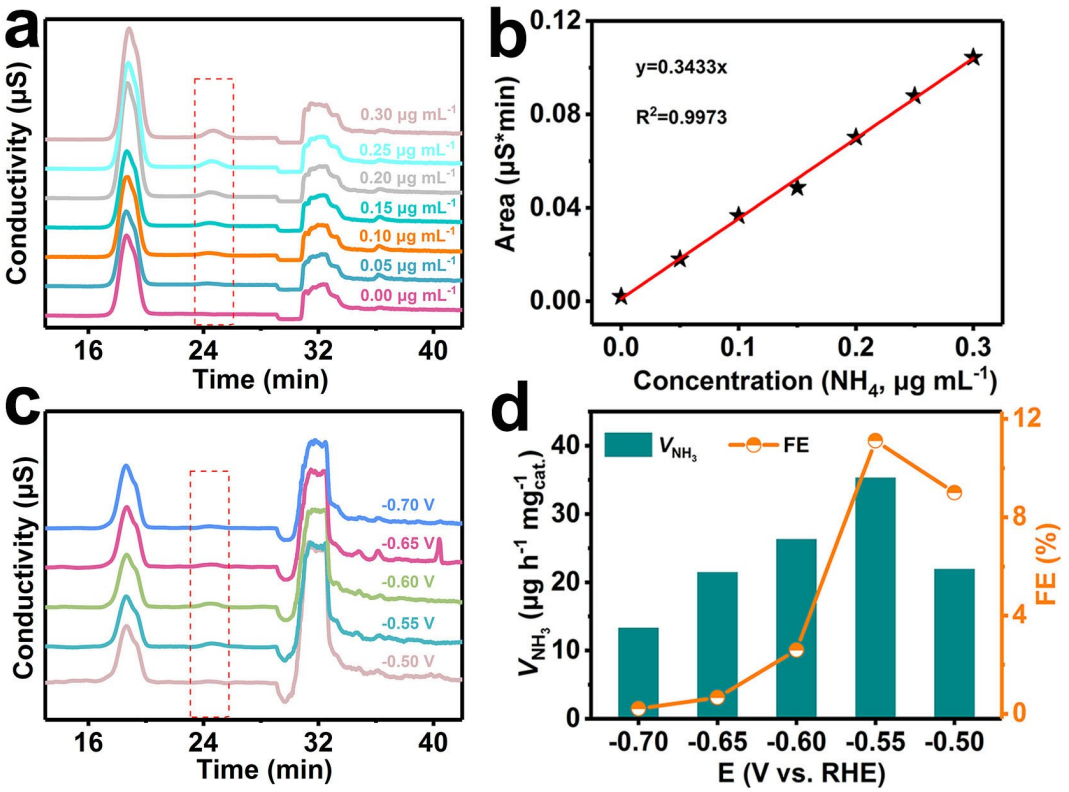

Fig. S8. (a) Ion chromatogram for the NH_4^+ ions. (b) Calibration curve used for estimation of NH_4^+. (c) Ion chromatogram for the electrolytes at a series of potentials after electrolysis for 2 h. (d) V_{NH3} and FEs for MnO_2-$Ti_3C_2T_x$/CP at corresponding potentials.

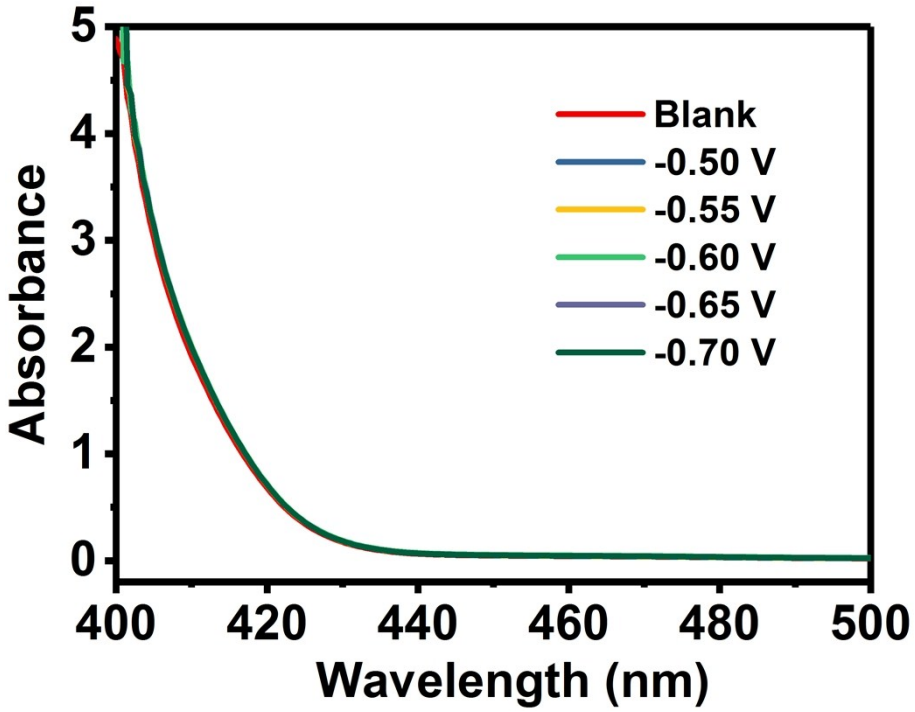

Fig. S9. UV–Vis spectra of the electrolyte estimated by the method of Watt and Chrisp before and after 2 h electrolysis in N_2 atmosphere at a series of potentials under ambient conditions.

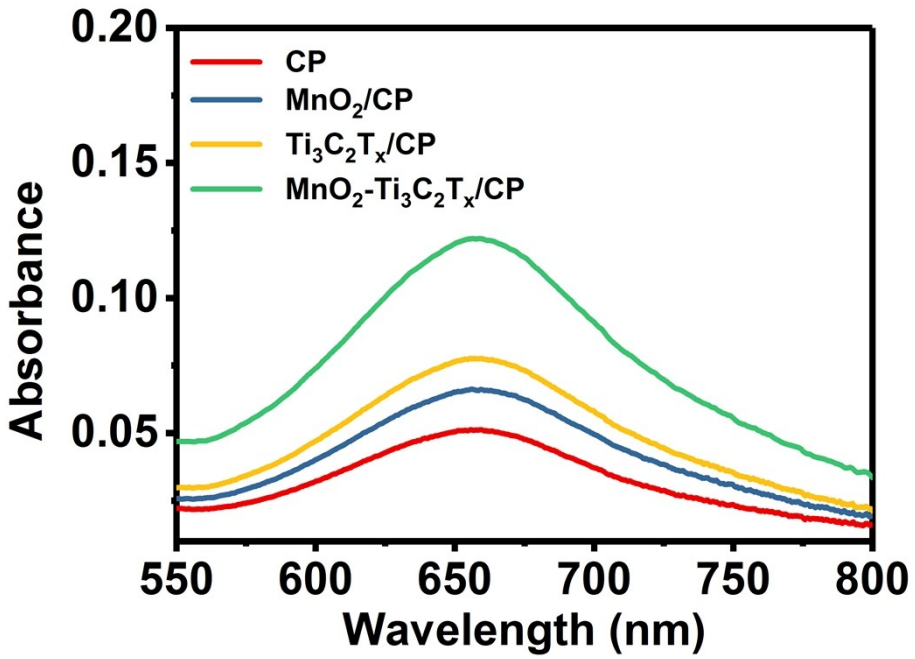

Fig. S10. UV–vis absorption spectra of the electrolytes stained with indophenol indicator after 2 h electrolysis in N_2-saturated solution at –0.55 V using CP, MnO_2/CP, $Ti_3C_2T_x$/CP, and MnO_2-$Ti_3C_2T_x$/CP as the working electrode, respectively.

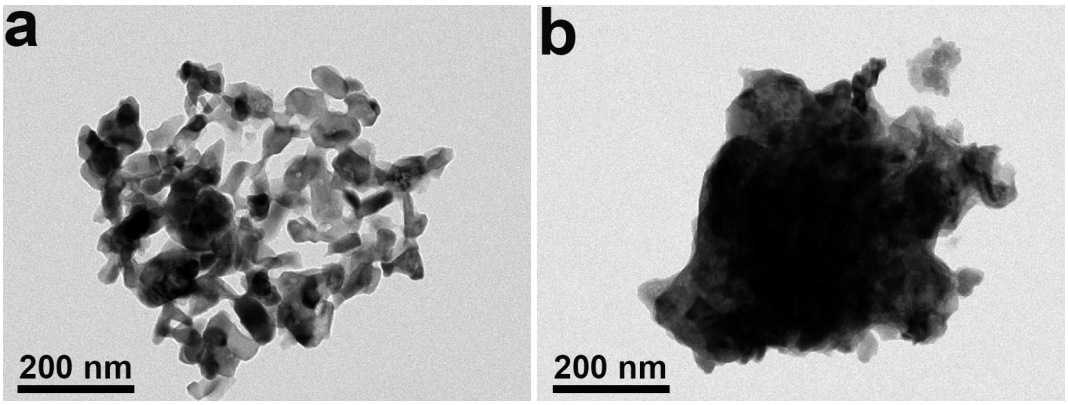

Fig. S11. TEM images of MnO_2 (a) before and (b) after 2 h electrolysis.

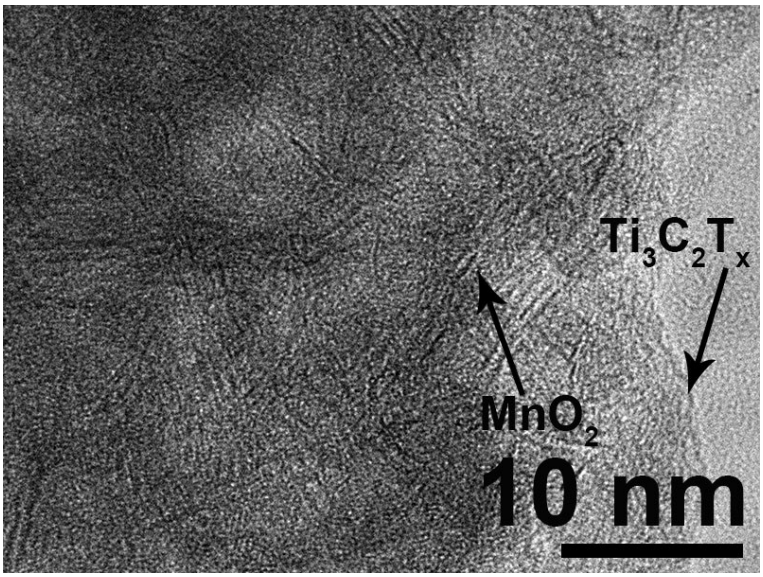

Fig. S12. TEM image of MnO_2-$Ti_3C_2T_x$ after long-term electrocatalysis.

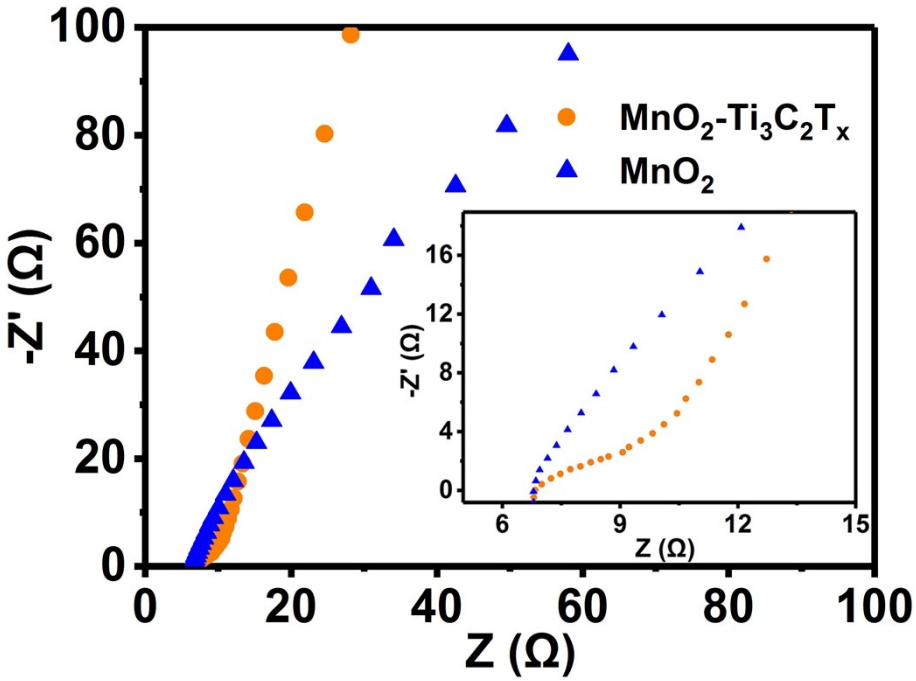

Fig. S13. Nyquist plots of MnO_2-$Ti_3C_2T_x$ and MnO_2.

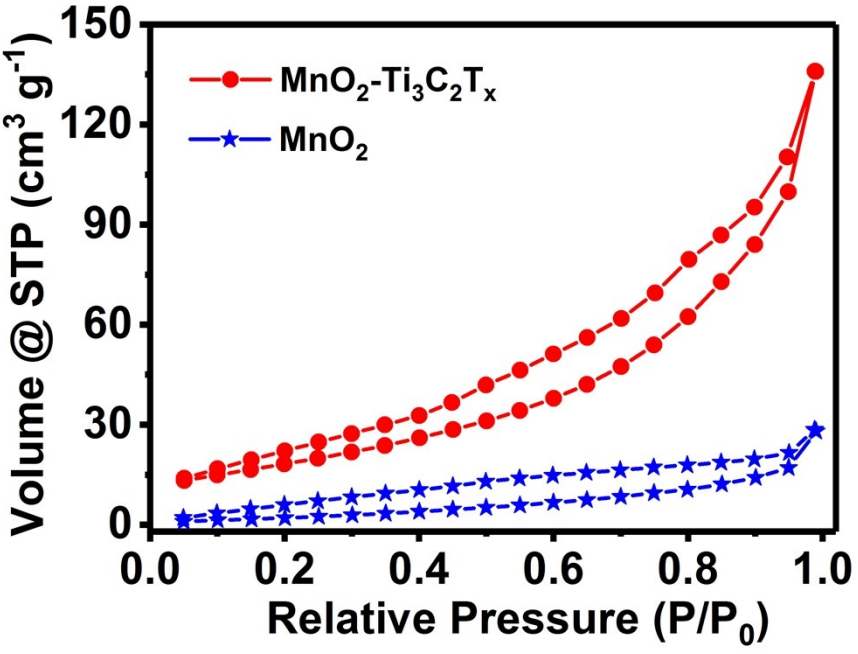

Fig. S14. N_2 adsorption-desorption isotherms of MnO_2-$Ti_3C_2T_x$ and MnO_2.

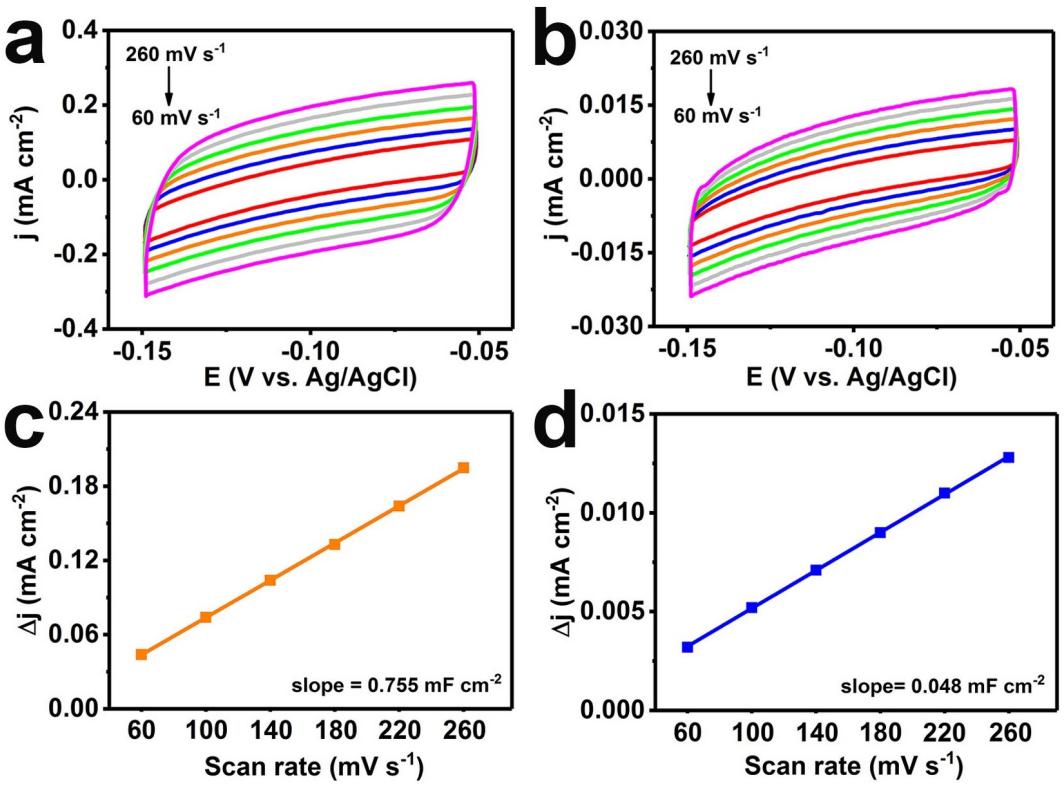

Fig. S15. CVs of (a) MnO_2-$Ti_3C_2T_x$/CP and (b) MnO_2/CP at various scan rates (60–260 mV s^{-1}) in the region of –0.05 to –0.15 V vs. Ag/AgCl. The capacitive current densities at –0.10 V vs. Ag/AgCl as a function of scan rates for (c) MnO_2-$Ti_3C_2T_x$/CP and (d) MnO_2/CP.

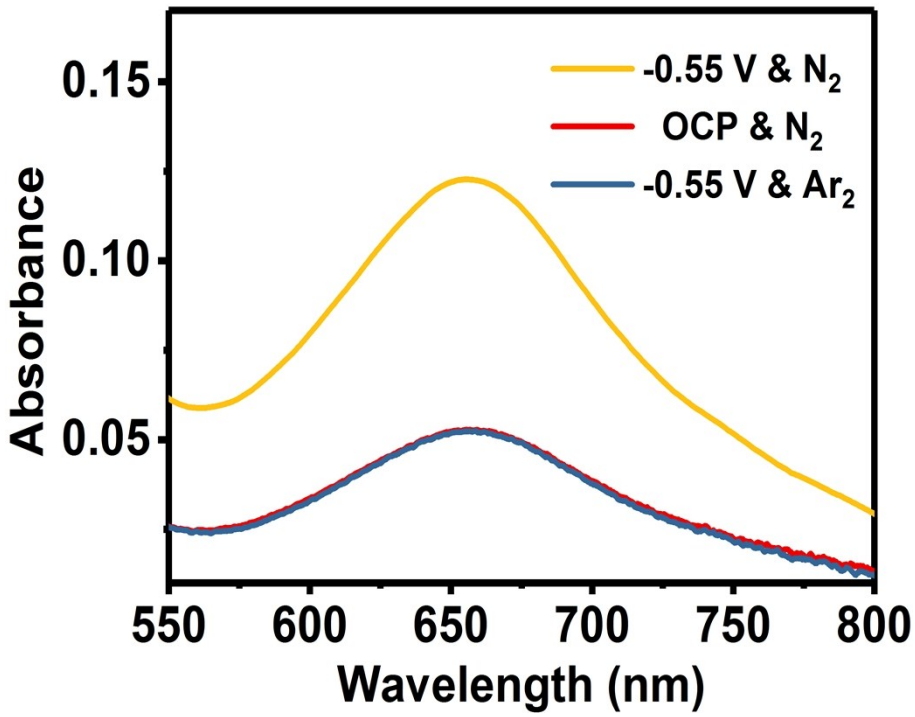

Fig. S16. UV-Vis absorption spectra of the electrolytes stained with indophenol indicator after 2 h electrolysis: in N_2-saturated solution at the potential of –0.55 V, N_2-saturated solution at an open-circuit potential and in Ar-saturated solution at –0.55 V.

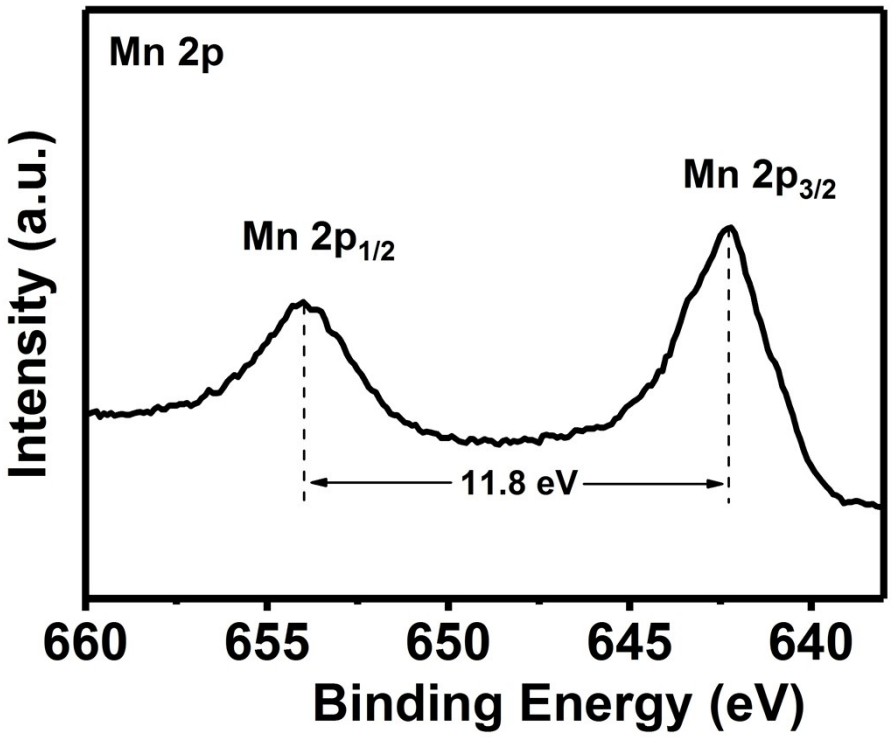

Fig. S17. XPS spectra for MnO_2-$Ti_3C_2T_x$ in the Mn 2p regions after long-term stability test.

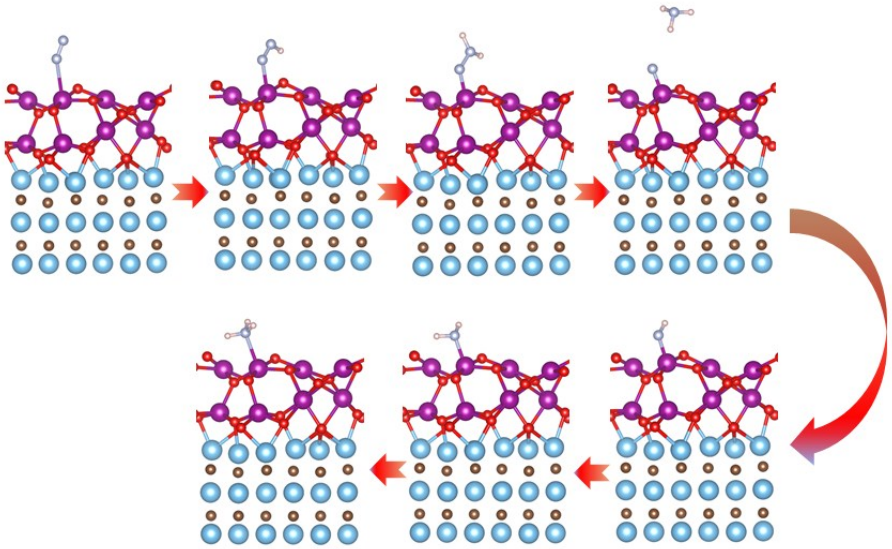

Fig. S18. Optimized structures of the intermediate species for the distal coordinate of MnO_2-$Ti_3C_2T_x$ composite.

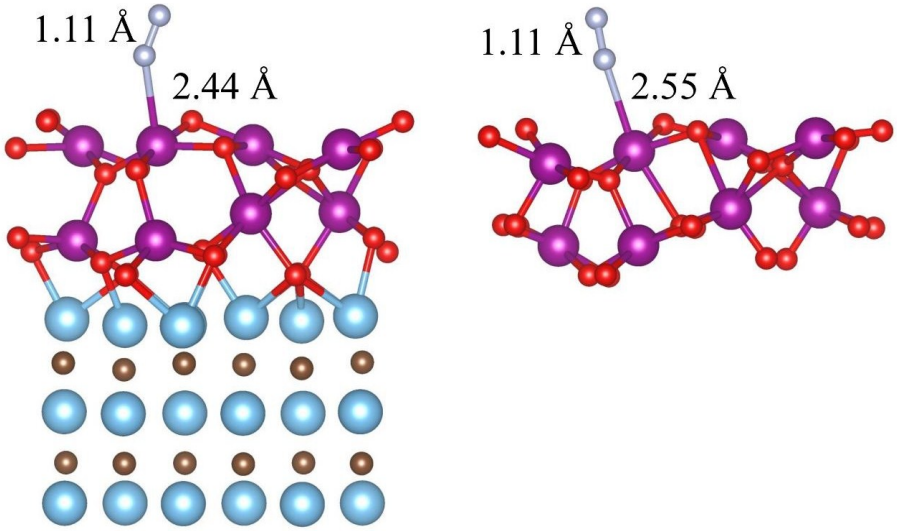

Fig. S19. Gibbs energy profile for the N_2 reduction process, performed on MnO_2(110)-MXene surface, through traditional distal pathway.

Table S1. Comparison of the NH_3 electrosynthesis activity for MnO_2-$Ti_3C_2T_x$ with other aqueous-based NRR electrocatalysts at ambient conditions.

Catalyst	Electrolyte	NH_3 yield rate	FE (%)	Ref.
MnO_2-$Ti_3C_2T_x$	**0.1 M HCl**	**34.12 μg h^{-1} $mg_{cat.}^{-1}$**	**11.39**	**This work**
$Ti_3C_2T_x/TiO_2$	0.1 M HCl	32.17 μg h^{-1} $mg_{cat.}^{-1}$	16.07	10
$Ti_3C_2T_x$ nanosheet	0.1 M HCl	20.4 μg h^{-1} $mg_{cat.}^{-1}$	9.3	11
Ag nanosheet	0.1 M HCl	4.62×10^{-11} mol s^{-1} cm^{-2}	4.8	12
C-TiO_2	0.1 M Na_2SO_4	16.22 μg h^{-1} $mg_{cat.}^{-1}$	1.84	13
MoS_2	0.1 M Na_2SO_4	8.8×10^{-11} mol s^{-1} cm^{-2}	1.17	14
MoN	0.1 M HCl	3.01×10^{-10} mol s^{-1} cm^{-2}	1.15	15
VN	0.1 M HCl	8.4×10^{-11} mol s^{-1} cm^{-2}	2.25	16
N-doped porous carbon	0.1 M HCl	15.7 μg h^{-1} $mg_{cat.}^{-1}$	1.45	17
hollow Cr_2O_3 microspheres	0.1 M Na_2SO_4	25.3 μg h^{-1} $mg_{cat.}^{-1}$	6.78	18
TiO_2-rGO	0.1 M Na_2SO_4	15.13 μg h^{-1} $mg_{cat.}^{-1}$	3.3	19
Au nanorods	0.1 M KOH	1.648 μg h^{-1} cm^{-2}	4	20
Fe_2O_3 nanorods	0.1 M Na_2SO_4	15.9 μg h^{-1} $mg_{cat.}^{-1}$	0.94	21
defect-rich MoS_2 nanoflower	0.1 M Na_2SO_4	29.28 μg h^{-1} $mg_{cat.}^{-1}$	8.34	22
Mn_3O_4 nanocube	0.1 M Na_2SO_4	11.6 μg h^{-1} $mg_{cat.}^{-1}$	3.0	23
Mn_3O_4 nanoparticles@rGO	0.1 M Na_2SO_4	17.4 μg h^{-1} $mg_{cat.}^{-1}$	3.52	24
MnO	0.1 M Na_2SO_4	1.11×10^{-10} mol s^{-1} cm^{-2}	8.02	25
PCN	0.1 M HCl	8.09 μg h^{-1} $mg_{cat.}^{-1}$	11.59	26
γ-Fe_2O_3	0.1 M KOH	12.5 nmol h^{-1} cm^{-2}	1.9	27
MoO_3	0.1 M HCl	29.43 μg h^{-1} $mg_{cat.}^{-1}$	1.9	28
MnO_2 with oxygen vacancies	0.1 M Na_2SO_4	1.63×10^{-10} mol s^{-1} cm^{-2}	11.40	29
Au nanorods	0.1 KOH	1.648 μg h^{-1} cm^{-2}	4	30
d-TiO_2	0.1 M HCl	1.24×10^{-10} mol s^{-1} cm^{-2}	9.17	31

References

1 M. Ghidiu, M. R. Lukatskaya, M. Q. Zhao, Y. Gogotsi and M. W. Barsoum, *Nature*, 2014, **516**, 78–81.

2 K. Maleski, C. E. Ren, M. Zhao, B. Anasori and Y. Gogotsi, *ACS Appl. Mater. Interfaces*, 2018, **29**, 24491–24498.

3 R. B. Rakhi, B. Ahmed, D. H. Anjum and H. N. Alshareef, *ACS Appl. Mater. Interfaces*, 2016, **29**, 18806–18814.

4 D. Zhu, L. Zhang, R. E. Ruther and R. J. Hamers, *Nat. Mater.*, 2013, **12**, 836–841.

5 G. W. Watt and J. D. Chrisp, *Anal. Chem.*, 1952, **24**, 2006–2008.

6 P. E. Blöchl, *Phys. Rev. B*, 1994, **50**, 17953–17979.

7 G. Kresse and D. Joubert, *Phys. Rev. B*, 1999, **9**, 1758–1775.

8 M. C. Payne, M. P. Teter, D. C. Allan, T. A. Arias and J. D. Joannopoulos, *Rev. Mod. Phys.*, 1992, **64**, 1045–1097.

9 F. Gong, Z. Ding, Y. Fang, C. Tong, D. Xia, Y. Lv, B. Wang, D. V. Papavassiliou, J. Liao and M. Wu, *ACS Appl. Mater. Interfaces*, 2018, **10**, 14614–14621.

10 Y. Fang, Z, Liu, J. Han, Z. Jin, Y. Han, F. Wang, Y. Niu, Y. Wu and Y. Xu, *Adv. Energy Mater.*, 2019, **9**, 1803406.

11 J. Zhao, L. Zhang, X. Xie, X. Li, Y. Yong, Q. Liu, W. Fang, X. Shi, G. Cui and X. Sun, *J. Mater. Chem. A*, 2018, **6**, 24031–24035.

12 H. Huang, L. Xia, X. Shi, A. M. Asiri and X. Sun, *Chem. Commun.*, 2018, **54**, 11427–11430.

13 K. Jia, Y. Wang, Q. Pan, B. Zhong, Y. Luo, G. Cui, X. Guo and X. Sun, *Nanoscale Adv.*, 2019, **1**, 961–964.

14 L. Zhang, X. Ji, X. Ren, Y. Ma, X. Shi, Z. Tian, A. M. Asiri, L. Chen, B. Tang and X. Sun, *Adv. Mater.*, 2018, **30**, 1800191.

15 L. Zhang, X. Ji, X. Ren, Y. Luo, X. Shi, A. M. Asiri, B. Zheng and X. Sun, *ACS Sustainable Chem. Eng.*, 2018, **6**, 9550–9554.

16 R. Zhang, Y. Zhang, X. Ren, G. Cui, A. M. Asiri, B. Zheng and X. Sun, *ACS*

Sustainable Chem. Eng., 2018, **6**, 9545–9549.

17 X. Yang, K. Li, D. Cheng, W. Pang, J. Lv, X. Chen, H. Zang, X. Wu, H. Tan, Y. Wang and Y. Li, *J. Mater. Chem. A*, 2018, **6**, 7762–7769.

18 Y. Zhang, W. Qiu, Y. Ma, Y. Luo, Z. Tian, G. Cui, F. Xie, L. Chen, T. Li and X. Sun, *ACS Catal.*, 2018, **8**, 8540–8544.

19 X. Zhang, Q. Liu, X. Shi, A. M. Asiri, Y. Luo, X. Sun and T. Li, *J. Mater. Chem. A*, 2018, ***6***, 17303–17306.

20 D. Bao, Q. Zhang, F. Meng, H. Zhong, M. Shi, Y. Zhang, J. Yan, Q. Jiang and X. Zhang, *Adv. Mater*., 2017, **29**, 1604799.

21 X. Xiang, Z. Wang, X. Shi, M. Fan and X. Sun, *ChemCatChem*., 2018, **20**, 4530–4535.

22 X. Li, T. Li, Y. Ma, Q. Wei, W. Qiu, H. Guo, X. Shi, P. Zhang, A. M. Asiri, L. Chen, B. Tang and X. Sun, *Adv. Energy Mater*., 2018, **8**, 1801357.

23 X. Wu, L. Xia, Y. Wang, W. Lu, Q. Liu, X. Shi and X. Sun, *Small*, 2018, **14**, 1803111.

24 H. Huang, F. Gong, Y. Wang, H. Wang, X. Wu, W. Lu, R. Zhao, H. Chen, X. Shi, A. M. Asiri, T. Li, Q. Liu and X. Sun, *Nano Res*., 2019, DOI: 10.1007/s12274-019-2352-5.

25 Z. Wang, F. Gong, L. Zhang, R. Wang, L. Ji, Q. Liu, Y. Luo, H. Guo, Y. Li, P. Gao, X. Shi, B. Li, B. Tang and X. Sun, *Adv. Sci*., 2018, **5**, 1801182.

26 C. Lv, Y. Qian, C. Yan, Y. Ding, Y. Liu, G. Chen and G. Yu, *Angew. Chem. Int. Ed.*, 2018, **57**, 10246−10250.

27 J. Kong, A. Lim, C. Yoon, J. H. Jang, H. C. Ham, J. Han, S. Nam, D. Kim, Y. Sung, J. Choi and H. S. Park, *ACS Sustainable Chem. Eng*., 2017, **5**, 10986–10995.

28 J. Han, X. Ji, X. Ren, G. Cui, L. Li, F. Xie, H. Wang, B. Li and X. Sun, *J. Mater. Chem. A*, 2018, **6**, 12974–12977.

29 L. Zhang, X. Xie, H. Wang, L. Ji, Y. Zhang, H. Chen, T. Li, Y. Luo, G. Cui and X. Sun, *Chem. Commun.*, 2019, **55**, 4627–4630.

30 D. Bao, Q. Zhang, F. Meng, H. Zhong, M. Shi, Y. Zhang, J. Yan, Q. Jiang and X. Zhang, *Adv. Mater*., 2017, **29**, 1604799.

31 L. Yang, T. Wu, R. Zhang, H. Zhou, L. Xia, X. Shi, H. Zheng, Y. Zhang and X. Sun,

Nanoscale, 2019, **11**, 1555–1562.